

# The impact of electron anisotropy on the polarization of the X-ray emission from black hole accretion disks and implications for the black hole X-ray binary 4U 1630–47

HENRIC KRAWCZYNSKI <sup>1</sup>, YAJIE YUAN <sup>2</sup>, ALEXANDER Y. CHEN <sup>2</sup>, NICOLE RODRIGUEZ CAVERO <sup>1</sup>, KUN HU <sup>1</sup>,  
EPHRAIM GAU <sup>1</sup>, JAMES F. STEINER <sup>3</sup>, AND MICHAL DOVČIAK <sup>4</sup>

<sup>1</sup>*Physics Department, McDonnell Center for the Space Sciences, and Center for Quantum Leaps, Washington University in St. Louis, St. Louis, MO 63130, USA*

<sup>2</sup>*Physics Department and McDonnell Center for the Space Sciences, Washington University in St. Louis, St. Louis, MO 63130, USA*

<sup>3</sup>*Harvard-Smithsonian Center for Astrophysics, 60 Garden Street, Cambridge, MA 02138, USA*

<sup>4</sup>*Astronomical Institute of the Czech Academy of Sciences, Boční II 1401/1, 14100 Praha 4, Czech Republic*

## ABSTRACT

The *Imaging X-ray Polarimetry Explorer (IXPE)* observations of the X-ray binary 4U 1630–47 in the high soft state revealed linear polarization degrees (PDs) rising from 6% at 2 keV to 10% at 8 keV. Explaining the results in the framework of the standard optically thick, geometrically thin accretion disk scenario requires careful fine-tuning of the relevant model parameters. We argue here that the emission of polarized Bremsstrahlung by anisotropic electrons in the accretion disk atmosphere can account for the overall high PDs and the increase of the PDs with energy. We discuss plasma and accretion effects that can generate electron anisotropies at a level required by the 4U 1630–47 results. We conclude by emphasizing that X-ray polarimetry affords us the opportunity to obtain information about the magnetization of the accretion disk atmosphere.

*Keywords:* Polarimetry (1278) — X-ray astronomy (1810) — Stellar mass black holes (1611)

## 1. INTRODUCTION

The *Imaging X-ray Polarimetry Explorer (IXPE)* (*IXPE*, Weisskopf et al. 2022) launched on Dec. 9, 2021 measured or constrained the polarization of the X-rays from several Black Hole X-ray Binaries (BHXRBs), including Cyg X-1 (Krawczynski et al. 2022; Dovciak et al. 2023), LMC X-1 (Podgorny et al. 2023), and 4U 1630–47 (Ratheesh et al. 2023; Rodriguez Caverio et al. 2023). In this paper, we will focus on the latter source, 4U 1630–47, a low-mass X-ray binary (LMXB) system showing recurrent outbursts every 2–3 years (Kuulkers et al. 1998; Capitanio et al. 2015). *IXPE* observed 4U 1630–47 in the High Soft State (HSS) (Ratheesh et al. 2023) and in the Steep Power Law (SPL) state (Rodriguez Caverio et al. 2023). The HSS observations are particularly interesting, as the HSS emission is dominated by the thermal multi-temperature emission from the optically thick, geometrically thin accretion disk (Shakura & Sun-

yaev 1973). X-ray polarimetric observations of BHXRBs thus give us a new way of testing the thin disk model which has been extremely successful in explaining the spectral observations of BHXRBs. The *IXPE* observations of 4U 1630–47 in the HSS revealed PDs increasing from ~6% at 2 keV to ~10% at 8 keV in the HSS (Ratheesh et al. 2023). Intriguingly, similar PDs were found in the SPL rising from ~5% at 2 keV to ~8% at 8 keV. Although the PDs were overall higher in the HSS than in the SPL state, the PDs varied as much during the HSS observations as their average between the HSS and the SPL observations. For both observations, the polarization angles (PAs) did not exhibit statistically significant variations with energy or in time.

Remarkably, the PDs measured in the HSS exceed those predicted by current state-of-the-art models (Li et al. 2009; Schnittman & Krolik 2009; Krawczynski & Beheshtipour 2022; Zhang et al. 2019; Taverna et al. 2020; Ratheesh et al. 2023). According to Chandrasekhar’s classical treatment of radiation transport in pure electron scattering atmospheres, scattering can create PDs reaching 11.71% for an observer at 90° inclination from the surface normal of the atmosphere (Chan-

Corresponding authors: H. Krawczynski (krawcz@wustl.edu), Yajie Yuan (yajiey@wustl.edu), Alexander Y. Chen (cyuran@wustl.edu).

drasekhar 1960). For the BHXRB 4U 1630–47, the observer is believed to view the accretion disk at  $\sim 65^\circ$  from the accretion disk normal and the axis of the binary. This inclination angle of the binary is consistent with the absence of eclipses and the presence of dips in the X-ray light curves (Tomsick et al. 1998; Kuulkers et al. 1998). For this inclination, Chandrasekhar’s theory predicts a much lower PD of 2.8%. Ratheesh et al. (2023) show that General Relativity (GR) effects close to the black hole (i.e., the parallel transport of the polarization direction of X-rays propagating through the black hole’s curved spacetime) and emission returning to the accretion disk and reflecting off the accretion disk reduce the predicted PDs by—depending on black hole spin and inclination—as much as 50%, rendering the maximal locally emitted PDs of 11.71% insufficient to explain the detected 6–10% PDs. Although the absorption of X-rays in the accretion disk can lead to slightly higher PDs and to a positive PD-energy correlation, the predicted PDs are still not high enough to explain the observations. Ratheesh et al. (2023) manage to fit the *IXPE* results by adopting a model with a low black hole spin value, extremely high locally emitted PDs from models with strong photospheric absorption, and the ad-hoc assumption of the emitting plasma outflowing with a velocity of 50% of the speed of light away from the accretion disk. The relativistic motion of the emitting plasma increases the PDs observed at moderate inclinations as X-rays emitted by the plasma at high inclinations reach the observer at lower inclinations owing to effect of relativistic aberration. The same authors discuss two other scenarios but find that they cannot explain the *IXPE* results: scattering off a wind tends to produce a constant polarization degree, contrary to the observational results (Veledina et al. 2023a); although slim disk models can generate increased PDs (West & Krawczynski 2023), they are again not high enough to account for the observed PDs.

We argue here that the previous studies neglected the possibility that the electron distribution function may exhibit anisotropies in the accretion disk atmosphere. As opposed to deep within the accretion flow, the accretion disk atmosphere can be weakly collisional, with scale height only a few times the electron collision mean free path. In such an environment, adiabatic invariance will adjust the parallel and perpendicular velocities with respect to the local magnetic field, leading to pressure anisotropy (e.g. Parker 1958). A common cause leading to such an anisotropy is large scale shearing motion which is prevalent in accretion disks. In moderate to high  $\beta$  plasmas, the pressure anisotropy can trigger fast-growing micro-scale mirror and firehose instabilities

that regulate the anisotropy to marginally stable levels, which is observed in the solar wind (Kunz et al. 2014).

This scenario is different from the one mentioned above of an outflowing plasma (Ratheesh et al. 2023). Both scenarios predict an anisotropic electron distribution for an observer co-rotating with the accretion disk. The scenario described here predicts substantially higher polarization degrees as the electrons are anisotropic in the rest frame of the emitting plasma (i.e., as seen by the much slower ions).

Motivated by the *IXPE* results, we ran Monte Carlo radiation transport calculations to evaluate the combined effects of Bremsstrahlung emission and scattering by anisotropic electrons for different ratios of the scattering to absorption cross sections. Our calculations show that electron anisotropies can boost the polarization by large amounts, easily reaching the  $\sim 20\%$  PDs of the locally emitted X-rays required to explain the 4U 1630–47 results. The rest of this letter is organized as follows. After describing the Monte Carlo radiation transport code in Sect. 2, we present the results from the simulations in Sect. 3. We conclude with a discussion of the plasma and accretion disk effects which might generate the required strong electron anisotropies in Sect. 4.

Note that solar flares are believed to emit strongly polarized Bremsstrahlung X-rays as well. We refer the reader to (Stackhouse & Kontar 2018, and references therein) for a discussion of the observational evidence and related theoretical treatments.

## 2. METHODS: RADIATION TRANSPORT IN AN ATMOSPHERE WITH ANISOTROPIC ELECTRONS

We demonstrate the effect of electron anisotropies on the polarization of the emergent X-rays based on Monte Carlo radiation transport simulations similar to those of Bai & Ramaty (1978); Jeffrey & Kontar (2011). Our code uses the scattering engine described in (Beheshtipour et al. 2017). Recent publications describing Monte Carlo simulations of Comptonizing plasmas include (Zhang et al. 2019; Krawczynski & Beheshtipour 2022; Kumar 2023).

In this letter, we model the electron anisotropy as a purely directional anisotropy without an associated temperature anisotropy. Future work might explore the observational signatures of different electron distributions in the three dimensional momentum space. We use two different parameterizations of the angular distribution of the electrons. The first parameterization assumes that the electrons are distributed with azimuthal symmetry around the surface normal of the atmosphere. The cosines  $\mu$  of the polar angles  $\theta$  of the electrons are

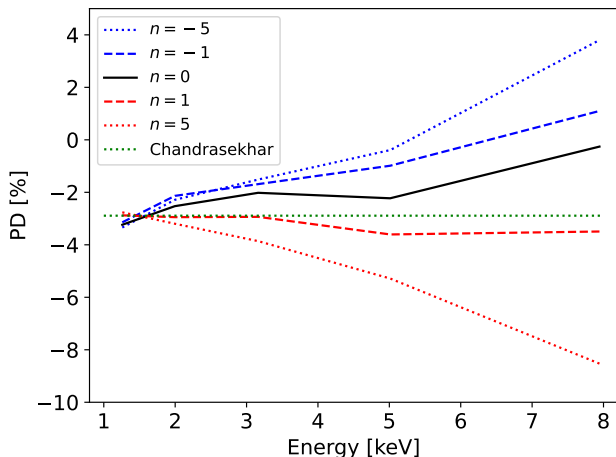


**Figure 1.** PDs produced by configuration #1 for a pure electron scattering atmosphere at temperature  $k_B T = 1$  keV for an observer at inclination  $i = 65^\circ$ . The lines show the results for  $n = -5$  (blue dotted line),  $n = -1$  (blue dashed line),  $n = 0$  (black solid line),  $n = 1$  (red dashed line) and  $n = 5$  (red dotted line). The green dotted line shows Chandrasekhar's result for reference.

assumed to follow the distribution:

$$p(\mu) \propto (\mu^2)^n \text{ for } n \geq 0, \text{ or} \quad (1)$$

$$p(\mu) \propto (1 - \mu^2)^{-n} \text{ for } n < 0. \quad (2)$$

Values  $n > 0$  ( $n < 0$ ) correspond to electron distributions with electrons moving preferentially perpendicular (parallel) to the atmosphere.

The second parameterization mimics gyrotropic electrons for magnetic field lines parallel to the surface of the atmosphere, for which the electron velocity distribution is isotropic perpendicular to the magnetic field, but the velocity distribution perpendicular to and parallel to the magnetic field are different. Such conditions are expected to develop in accretion disks as shearing motions are likely to generate a dominant toroidal magnetic field. In this case, we also use the probability distributions of Equations (1) and (2), but with  $\mu$  being the cosine of the angle between the electron velocity and the  $x$ -axis parallel to the atmosphere (corresponding to the direction of the magnetic field). We call the index  $m$  instead of  $n$  to clearly distinguish this setup from the one above. We collect photons leaving the atmosphere within  $\pm 10^\circ$  azimuthal angles from the  $x$ -axis ( $y$ -axis) to get the polarization for observers viewing the atmosphere along the direction of the  $x$ -axis ( $y$ -axis).

Our code runs in two configurations. Configuration #1 is used to study the polarization of X-rays emitted

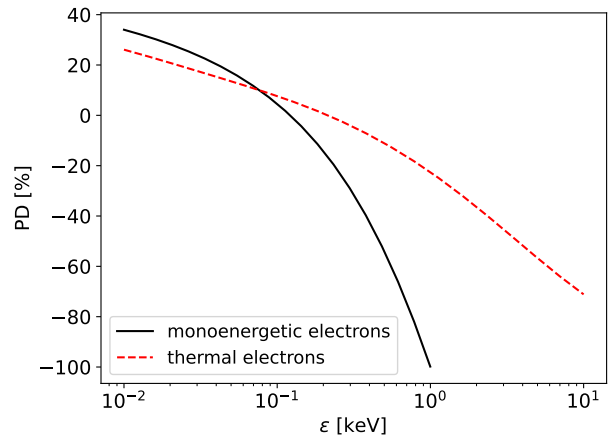


**Figure 2.** PDs produced by mono-directional electrons with kinetic energy of 1 keV (solid black line) and at a temperature of  $k_B T = 1$  keV (dashed red line) as a function of the photon energy for a viewing angle of  $65^\circ$  from the direction of the electron beam. The PD is positive for electric field vectors perpendicular to the electron beam, and negative for electric field vectors parallel to the beam.

by pure scattering atmospheres with anisotropic electrons. The photons are emitted at the bottom of the atmosphere extending from  $z = -5 l_{sc}$  to  $z = 0$  with  $l_{sc}$  being the scattering mean free path. We set the polarization of the emitted photons to 0 to clearly see the effect of the scatterings on the photon polarization.

Photons scatter off electrons drawn from a Maxwell-Jüttner distribution of temperature  $T$ . The code uses four wave-vectors  $k^\mu = (E, E\vec{n})$  to keep track of the energy  $E$  and the direction  $\vec{n}$  of a photon. The code keeps track of the photon's linear polarization with the help of a parameter tracking the PD, and the polarization vector  $f^\mu = (0, \vec{f})$  with  $|\vec{f}| = 1$  encoding the electric field polarization direction (Misner et al. 2018). The Compton scattering is effected by Lorentz transforming  $k^\mu$  and  $f^\mu$  into the scattering electron's rest frame. After drawing a random direction of the scattered photon, we construct the Stokes vector of the incoming photon referenced to the plane spanned by the wave vectors of the incoming and outgoing photon. The Stokes vector of the outgoing photon is calculated by multiplying the Stokes vector of the incoming photon with Fano's fully relativistic scattering matrix (Fano 1957; McMaster 1961; Beheshtipour et al. 2017). A rejection algorithm uses the Stokes- $I$  parameter of the scattered photon to account for the energy and scattering angle dependence of the Klein-Nishina cross section. The scattering changes the photon energy in the electron rest frame according to

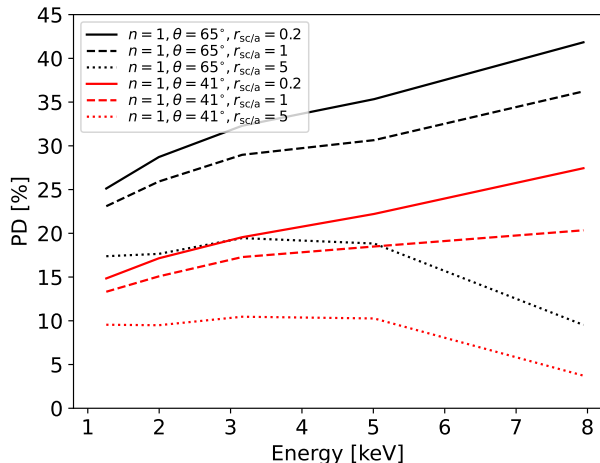


**Figure 3.** PDs produced by configuration #2 by thermal 1 keV electrons moving preferentially perpendicular to the atmosphere ( $n = 1$ ) for observers at  $i = 65^\circ$  (black lines) and  $i = 41^\circ$  (red lines). For each color, the different lines show the results for different scattering to absorption cross section ratios:  $r_{sc/a} = 0.2$  (solid lines), 1 (dashed lines), and 5 (dotted lines). The polarization is positive, i.e., perpendicular to the atmosphere.

Compton’s equation. The Stokes vector is subsequently used to infer the PD and polarization direction  $\hat{f}$  of the scattered photon. In the last step, the wave and polarization vectors are transformed back into the plasma frame. We switched off all relativistic effects (change of electron energy, Klein-Nishina cross section, scattering probability as function of the angle between electron velocity and photon wave vector, see Beheshtipour et al. 2017) to verify that the code reproduces Chandrasekhar’s results. The Comptonization code was furthermore cross-checked in the deep Klein-Nishina regime against the MONK code (W. Zhang, private communication, 2022).

Configuration #2 is used to study the impact of the polarized Bremsstrahlung emission, photon absorption, and Compton scattering on the polarization of the emergent emission. We simulate a 5-absorption-length-deep atmosphere at (electron) temperature  $T$ . The relative importance of emission and scattering is parameterized by the ratio  $r_{sc/a}$  of the absorption to scattering cross sections, and we use the parameters  $n$  and  $m$  to characterize the electron anisotropy. Bremsstrahlung photons are emitted uniformly throughout the atmosphere. The PD and polarization angle are generated making use of the relativistic cross sections  $\sigma_{II}$  and  $\sigma_{III}$  for the emission of photons polarized parallel and perpendicular to the plane defined by the electron and photon

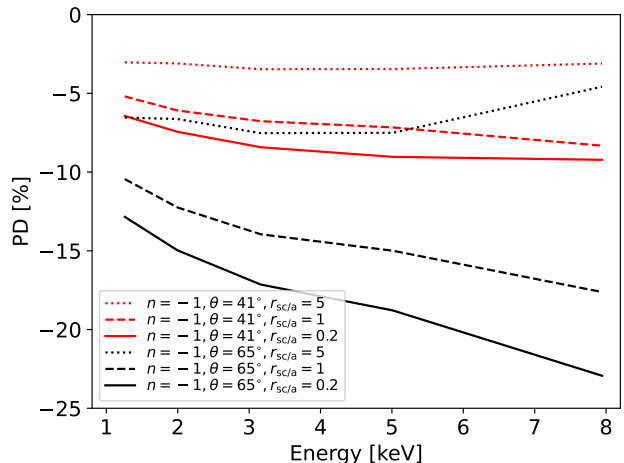


**Figure 4.** Same as the red and black lines in Fig. 3 but for electrons moving preferentially parallel to the atmosphere ( $n = -1$ ). The polarization is negative, i.e. parallel to the atmosphere in all cases.

velocity vectors derived by Gluckstern & Hull (1953) in the first Born approximation. Note that Equations (4.2) and (4.3) of (Gluckstern & Hull 1953) are correct up to a typo (multiplication instead of subtraction at the beginning of the last line their Equation (4.3)) that Gluckstern acknowledged in a private communication mentioned in (Bai & Ramaty 1978). The reproductions of these equations in (Bai & Ramaty 1978) include errors as do those in (Komarov et al. 2016). The latter authors give the Bremsstrahlung cross sections in convenient form, but their Equation (16) for  $L$  includes a factor of 2 that should be dropped. In our code, photons propagate until they are absorbed, scatter, or escape the atmosphere. The Compton scatterings are simulated as explained for configuration #1.

Photons escaping the atmosphere are sorted into 6 bins in the cosine of the inclination of the observer  $\mu_{obs}$  and in 5 bins in energy, and the Stokes parameters within each bin are summed. Owing to the symmetry of the plane parallel atmosphere, Stokes- $U$  vanishes. We denote electric field polarizations perpendicular to the atmosphere as positive polarization ( $PD=Q/I >0$ ), and polarizations parallel to the atmosphere as negative polarization ( $PD=Q/I <0$ ).

### 3. RESULTS: POLARIZATION FROM ANISOTROPIC ELECTRONS

We present here the results from simulations performed for a plasma temperature of 1 keV, which roughly equals the temperature of the upper layers of the photosphere of the inner portion of the accretion

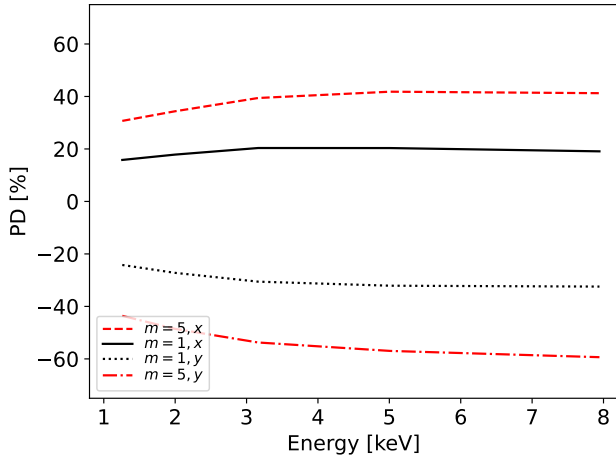


**Figure 5.** Polarization from electrons with  $m = +1$  (black lines) and  $m = +5$  (red lines) as seen for an  $i = 65^\circ$  observer viewing the atmosphere along the direction of the symmetry  $x$ -axis (dashed and solid lines) and perpendicular to it in the plane of the atmosphere ( $y$ -axis, dotted and dash-dotted lines) for  $r_{sc/a} = 1$ .

disk of 4U 1630–47 during the *IXPE* observations (accounting for a spectral hardening factor of 1.8).

The black solid line in Figure 1 shows the polarization from configuration #1 (pure electron scattering atmosphere) for an isotropic electron distribution ( $n = 0$ ). Interestingly, the strength of the polarization decreases with energy, as on average more scatterings are needed to scatter thermally emitted lower-energy photons to higher energies. The red lines show that electrons moving preferentially perpendicular to the atmosphere ( $n > 0$ ) make the polarization parallel to the atmosphere stronger. The blue lines give the results for electron moving preferentially parallel to the atmosphere ( $n < 0$ ) creating polarization perpendicular to the atmosphere which can win over the parallel polarization at higher energies.

The results above show that anisotropic Compton scattering can increase the PDs. In the next step, we will show that the inclusion of absorption and Bremsstrahlung can give rise to much higher PDs. Figure 2 shows the polarization of the Bremsstrahlung from mono-directional 1 keV electrons. At the lowest energies ( $\lesssim 0.1$  keV) the emission is polarized perpendicular to the direction of the electrons, as the emission comes predominantly from small deflections of the electrons. At higher energies, the emission is polarized parallel to the electron beam, as the emission comes mostly from the longitudinal acceleration of the electrons. The parallel polarization reaches 100% in the limit that the

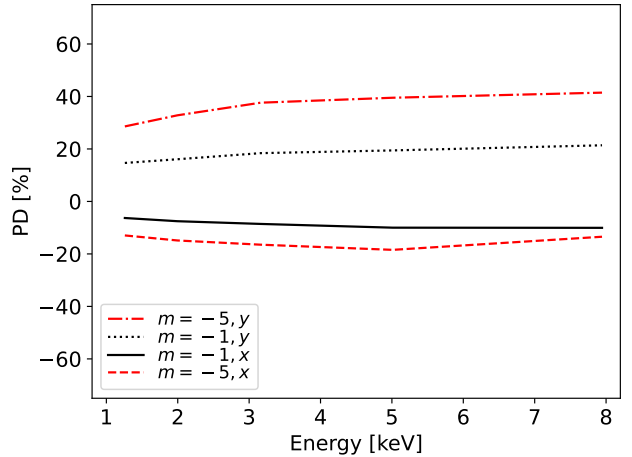


**Figure 6.** Polarization from electrons with  $m = -1$  (black lines) and  $m = -5$  (red lines) as seen for an  $i = 65^\circ$  observer viewing the atmosphere along the direction of the symmetry  $x$ -axis (solid and dashed lines) and perpendicular to it in the plane of the atmosphere ( $y$ -axis, dash-dotted and dotted lines) for  $r_{sc/a} = 1$ .

photon energy equals the electron energy. A similar switch from perpendicular to parallel polarization occurs for the Bremsstrahlung emission from monodirectional electrons at a temperature of  $k_B T = 1$  keV, see Fig. 2, dashed red line.

Figures 3 and 4 show the results from the radiative transport simulations of configuration #2, where the emergent PD depends on the combined effect of polarized Bremsstrahlung emission, photon absorption, and photon scattering. Figure 3 shows that electrons moving preferentially perpendicular to the disk with  $n = 1$  can produce  $65^\circ$ -inclination PDs increasing from 2 to 8 keV from 25% to 40% if absorption dominates over scattering ( $r_{sc/a} = 0.2$ ). Although the polarization is weaker when the electrons move preferentially parallel to the disk with  $n = -1$  (Fig. 4), the PDs can still be sufficiently high to explain the 4U 1630–47 results.

Figures 5 and Figures 6 present the results for electron direction distributions symmetric around the  $x$ -axis parallel to the surface of the atmosphere. For both types of distributions ( $m > 0$  and  $m < 0$ ), the polarization direction depends on the viewing direction. The forward-backward anisotropies with  $m > 0$  tend to produce stronger polarizations than the toroidal anisotropies with  $m < 0$ .

#### 4. DISCUSSION

Our calculations demonstrate that polarized Bremsstrahlung can produce large net-PDs as long as

Compton scatterings do not suppress the polarization towards Chandrasekhar’s classical results. For electron anisotropies of order unity, the net PD can easily reach the  $\sim 20\%$  levels required for explaining the observed 6%-10% PDs of the 2-8 keV emission from 4U 1630–47. Work is in progress to embed the results presented above into the `kerrC` code that simulates the emission from all parts of an accretion disk of a spinning Kerr black hole and ray traces the emission to the observer (Krawczynski & Beheshtipour 2022). Simulations for a wide range of black hole spin parameters and accretion rates would allow us to fit the *IXPE* observations of 4U 1630–47 and other sources observed in the HSS.

In the thermal state, the deeper layers of the accretion disk are highly collisional and emit blackbody emission. The radiation then passes through the accretion disk atmosphere where it is reprocessed owing to bound-bound, bound-free, and free-free absorption processes and Compton scatterings. The electrons cool by Bremsstrahlung emission and inverse Compton processes. The net outcome of the absorption, scattering, and emission processes is a reprocessed quasi-thermal emission at a higher temperature than in the mid-disk, but with a lower surface brightness than blackbody emission at this temperature (e.g., Shimura & Takahara 1993, 1995; Taverna et al. 2021). We argue in this letter that the reprocessing of the emission in the atmosphere can generate the strong polarization of the emerging X-rays.

If the density in the accretion disk atmosphere is low enough such that the scale height is only a few times the electron collisional mean free path, the plasma is weakly collisional. Since the electron-electron collision rate is similar to the electron-ion collision rate which determines the efficiency of Bremsstrahlung emission (e.g., Kulsrud 2005; Thorne & Blandford 2017), the electrons in the atmosphere are weakly collisional while the ions can be collisionless. In this regime, the electron and ion distributions can develop anisotropy: their temperature/pressure parallel and perpendicular to the magnetic field can be different. The anisotropy is typically driven by the change of the magnetic field. For example, the differential rotation of the gas in the disk atmosphere leads to the amplification of the toroidal magnetic field. In the absence of collisions, particles will conserve their adiabatic invariants, therefore, the pressure perpendicular to the magnetic field  $P_{\perp}$  and parallel to the magnetic field  $P_{\parallel}$  evolve separately according to:

$$\frac{d}{dt} \left( \frac{P_{\perp}}{\rho B} \right) = 0, \quad \frac{d}{dt} \left( \frac{P_{\parallel} B^2}{\rho^3} \right) = 0, \quad (3)$$

where  $\rho$  is the plasma density,  $B$  is the magnetic field (Chew et al. 1956). The shear motion increasing  $B$  without changing  $\rho$  will lead to  $P_{\perp} > P_{\parallel}$ . On the other hand, if  $B$  decreases,  $P_{\parallel} > P_{\perp}$  develops instead.

The anisotropy can be limited by a few processes. Firstly, collisions will tend to isotropize the particle distribution. As a rough estimation,

$$\frac{P_{\perp} - P_{\parallel}}{P} \sim \frac{1}{\nu} \frac{1}{B} \frac{dB}{dt} \sim \frac{u}{v_{\text{th}} L_u}, \quad (4)$$

where  $\nu$  is the collision rate,  $\lambda$  is the collisional mean free path,  $v_{\text{th}}$  is the thermal velocity of plasma particles,  $u$  is the (shear) flow velocity and  $L_u$  is the length scale over which the velocity varies (Komarov et al. 2016). In the disk atmosphere, the orbital velocity  $u$  is close to Keplerian,  $u \gg v_{\text{th}}$ , and  $L_u$  is a few times of the collisional mean free path  $\lambda$  in the weakly collisional regime, therefore it is possible to get order unity anisotropy. Other processes that can limit the anisotropy include kinetic instabilities caused by the pressure anisotropy itself: the fire hose instability can develop when  $P_{\parallel}/P_{\perp} > (1 - 2/\beta_{\parallel})^{-1}$ , and a mirror instability can develop in the opposite regime  $P_{\perp}/P_{\parallel} > 1 + 1/\beta_{\perp}$ , where  $\beta_{\parallel} = P_{\parallel}/(B^2/8\pi)$  and  $\beta_{\perp} = P_{\perp}/(B^2/8\pi)$  (e.g., Kunz et al. 2014). These instabilities lead to microscopic fluctuations that can scatter particles, leading to collisional effects that limit the pressure anisotropy at the threshold values. The amount of anisotropy will be small if  $\beta_{\perp}, \beta_{\parallel} \gg 1$ , e.g. inside the accretion disk. However, in the atmosphere, the beta parameters can be relatively small,  $\beta \lesssim$  a few. When  $\beta_{\parallel} < 2$ , the fire hose instability can no longer develop and  $P_{\parallel}/P_{\perp}$  is unlimited; for the mirror boundary, when  $\beta_{\perp} < 1$ , the limiting value of  $P_{\perp}/P_{\parallel}$  becomes larger than 2. The discussion shows that electron anisotropies of order unity are not guaranteed but can develop.

Since the electron anisotropy evolves with the local coherent magnetic field, it is closely linked to the geometry and evolution of the global magnetic field. Most General Relativistic Magnetohydrodynamic (GRMHD) simulations of black hole accretion find that any initially weak magnetic field in the accretion disk is sheared and amplified to be predominantly toroidal (e.g., Hirose et al. 2004). This appears to be the case for both the standard and normal evolution (SANE) and magnetically arrested disks (MAD) (e.g. Begelman et al. 2022), except for the region close to the event horizon and the jet base, where significant amount of poloidal field may exist. The second parameterization described in Section 2 (denoted by index  $m$ ) corresponds to electron anisotropy with respect to a predominantly toroidal magnetic field. If shear motion amplifies the magnetic field in the accretion disk and in the accretion disk atmosphere, the out-

come  $P_{\perp} > P_{\parallel}$  corresponds to the polarization signature of Fig. 6. The  $m = -1$  case corresponds to  $P_{\perp}/P_{\parallel} = 2$  and  $m = -5$  case has  $P_{\perp}/P_{\parallel} = 6$ , which may be realized in a weakly collisional, low beta plasma. The polarization perpendicular to the atmosphere would be stronger than the polarization parallel to the atmosphere and would likely dominate the overall polarization of the signal. The  $P_{\perp} < P_{\parallel}$  case would produce the opposite outcome of Fig. 5. In this scenario,  $m = 1$  gives  $P_{\parallel}/P_{\perp} = 3$  and  $m = 5$  would mean  $P_{\parallel}/P_{\perp} = 11$ . Unfortunately, for the specific case of 4U 1630–47 for which the strong HSS polarization indicates strong electron anisotropies, we do not have independent information about the orientation of the binary system or the accretion disk in the sky. Thus, even though the electric field polarization gives us the preferred direction of the electron motion, we cannot relate this to the orientation of the accretion disk. In contrast, for the source Cyg X-1, the detected radio jet (Stirling et al. 2001) constrains the accretion disk orientation in the sky to be perpendicular to the jet. In this case, detailed modeling of HSS data should enable us to observationally determine if  $P_{\perp} > P_{\parallel}$  or  $P_{\perp} < P_{\parallel}$ .

As mentioned above, the *IXPE* observations of 4U 1630–47 in the HSS and SPL states revealed similar polarization properties in both states (Rodriguez Cavero et al. 2023). These results can possibly be explained in the framework of the emission model discussed here. The transition from the HSS to the SPL state would merely require the emergence of a non-

thermal tail of the electron distribution. A somewhat stronger Comptonization of the Bremsstrahlung emission could account for the somewhat smaller PDs but identical polarization direction of the emission. The relative constancy of the polarization degree would then argue for a rather similar overall disk configuration in the HSS and SPL states, i.e., similar disk truncation radii. Given the high PDs that Bremsstrahlung can produce, it might be worthwhile to evaluate if it may impact the polarization of the hard state emission of the sources Cyg X-1 (Krawczynski et al. 2022) and Cyg X-3 (Veledina et al. 2023b).

*Acknowledgments:* H.K. thanks Banafsheh Beheshtipour for the code of the original Compton scattering engine. H.K., N.R.C., and K.H. acknowledge extremely pleasant and fruitful discussions with Michal Dovčiak, Jack Steiner, and Javier García, as well as with the entire *IXPE* stellar mass black hole science working group. H.K., N.R.C., and K.H. acknowledge NASA support through the grants NNX16AC42G, 80NSSC20K0329, 80NSSC20K0540, NAS8-03060, 80NSSC21K1817, 80NSSC22K1291, and 80NSSC22K1883. A.C. and Y.Y. acknowledge support from NSF grants DMS-2235457 and AST-2308111. A.C. also acknowledges NASA support from grant 80NSSC21K2027. Y.Y. also acknowledges support by the Multimessenger Plasma Physics Center (MPPC), NSF grant PHY-2206608. The Washington University authors acknowledge support from the McDonnell Center for the Space Sciences.

## REFERENCES

- Bai, T., & Ramaty, R. 1978, *ApJ*, 219, 705, doi: [10.1086/155830](https://doi.org/10.1086/155830)
- Begelman, M. C., Scepi, N., & Dexter, J. 2022, *MNRAS*, 511, 2040, doi: [10.1093/mnras/stab3790](https://doi.org/10.1093/mnras/stab3790)
- Beheshtipour, B., Krawczynski, H., & Malzac, J. 2017, *ApJ*, 850, 14, doi: [10.3847/1538-4357/aa906a](https://doi.org/10.3847/1538-4357/aa906a)
- Capitaniao, F., Campana, R., De Cesare, G., & Ferrigno, C. 2015, *MNRAS*, 450, 3840, doi: [10.1093/mnras/stv687](https://doi.org/10.1093/mnras/stv687)
- Chandrasekhar, S. 1960, *Radiative Transfer* (New York: Dover Publications)
- Chew, G. F., Goldberger, M. L., & Low, F. E. 1956, *Proceedings of the Royal Society of London Series A*, 236, 112, doi: [10.1098/rspa.1956.0116](https://doi.org/10.1098/rspa.1956.0116)
- Dovciak, M., Steiner, J. F., Krawczynski, H., & Svoboda, J. 2023, *The Astronomer’s Telegram*, 16084, 1
- Fano, U. 1957, *Reviews of Modern Physics*, 29, 74, doi: [10.1103/RevModPhys.29.74](https://doi.org/10.1103/RevModPhys.29.74)
- Gluckstern, R. L., & Hull, M. H. 1953, *Physical Review*, 90, 1030, doi: [10.1103/PhysRev.90.1030](https://doi.org/10.1103/PhysRev.90.1030)
- Hirose, S., Krolik, J. H., De Villiers, J.-P., & Hawley, J. F. 2004, *ApJ*, 606, 1083, doi: [10.1086/383184](https://doi.org/10.1086/383184)
- Jeffrey, N. L. S., & Kontar, E. P. 2011, *A&A*, 536, A93, doi: [10.1051/0004-6361/201117987](https://doi.org/10.1051/0004-6361/201117987)
- Komarov, S. V., Khabibullin, I. I., Churazov, E. M., & Schekochihin, A. A. 2016, *MNRAS*, 461, 2162, doi: [10.1093/mnras/stw1370](https://doi.org/10.1093/mnras/stw1370)
- Krawczynski, H., & Beheshtipour, B. 2022, *ApJ*, 934, 4, doi: [10.3847/1538-4357/ac7725](https://doi.org/10.3847/1538-4357/ac7725)
- Krawczynski, H., Muleri, F., Dovčiak, M., et al. 2022, *Science*, 378, 650, doi: [10.1126/science.add5399](https://doi.org/10.1126/science.add5399)
- Kulsrud, R. M. 2005, *Plasma physics for astrophysics* (Princeton, N.J.: Princeton University Press)
- Kumar, N. 2023, *arXiv e-prints*, arXiv:2307.08023, doi: [10.48550/arXiv.2307.08023](https://doi.org/10.48550/arXiv.2307.08023)

- Kunz, M. W., Schekochihin, A. A., & Stone, J. M. 2014, *PhRvL*, 112, 205003, doi: [10.1103/PhysRevLett.112.205003](https://doi.org/10.1103/PhysRevLett.112.205003)
- Kuulkers, E., Wijnands, R., Belloni, T., et al. 1998, *ApJ*, 494, 753, doi: [10.1086/305248](https://doi.org/10.1086/305248)
- Li, L.-X., Narayan, R., & McClintock, J. E. 2009, *ApJ*, 691, 847, doi: [10.1088/0004-637X/691/1/847](https://doi.org/10.1088/0004-637X/691/1/847)
- McMaster, W. H. 1961, *Reviews of Modern Physics*, 33, 8, doi: [10.1103/RevModPhys.33.8](https://doi.org/10.1103/RevModPhys.33.8)
- Misner, C. W., Thorne, K. S., Wheeler, J. A., & Kaiser, D. I. 2018, *Gravitation*
- Parker, E. N. 1958, *Physical Review*, 109, 1874, doi: [10.1103/PhysRev.109.1874](https://doi.org/10.1103/PhysRev.109.1874)
- Podgorny, J., Marra, L., Muleri, F., et al. 2023, arXiv e-prints, arXiv:2303.12034, doi: [10.48550/arXiv.2303.12034](https://doi.org/10.48550/arXiv.2303.12034)
- Ratheesh, A., Dovčiak, M., Krawczynski, H., et al. 2023, arXiv e-prints, arXiv:2304.12752, doi: [10.48550/arXiv.2304.12752](https://doi.org/10.48550/arXiv.2304.12752)
- Rodriguez Caverro, N., Marra, L., Krawczynski, H., et al. 2023, arXiv e-prints, arXiv:2305.10630, doi: [10.48550/arXiv.2305.10630](https://doi.org/10.48550/arXiv.2305.10630)
- Schnittman, J. D., & Krolik, J. H. 2009, *ApJ*, 701, 1175, doi: [10.1088/0004-637X/701/2/1175](https://doi.org/10.1088/0004-637X/701/2/1175)
- Shakura, N. I., & Sunyaev, R. A. 1973, *A&A*, 24, 337
- Shimura, T., & Takahara, F. 1993, *ApJ*, 419, 78, doi: [10.1086/173460](https://doi.org/10.1086/173460)
- . 1995, *ApJ*, 445, 780, doi: [10.1086/175740](https://doi.org/10.1086/175740)
- Stackhouse, D. J., & Kontar, E. P. 2018, *A&A*, 612, A64, doi: [10.1051/0004-6361/201730708](https://doi.org/10.1051/0004-6361/201730708)
- Stirling, A. M., Spencer, R. E., de la Force, C. J., et al. 2001, *MNRAS*, 327, 1273, doi: [10.1046/j.1365-8711.2001.04821.x](https://doi.org/10.1046/j.1365-8711.2001.04821.x)
- Taverna, R., Marra, L., Bianchi, S., et al. 2021, *MNRAS*, 501, 3393, doi: [10.1093/mnras/staa3859](https://doi.org/10.1093/mnras/staa3859)
- Taverna, R., Zhang, W., Dovčiak, M., et al. 2020, *MNRAS*, 493, 4960, doi: [10.1093/mnras/staa598](https://doi.org/10.1093/mnras/staa598)
- Thorne, K. S., & Blandford, R. D. 2017, *Modern Classical Physics: Optics, Fluids, Plasmas, Elasticity, Relativity, and Statistical Physics* (Princeton University Press)
- Tomsick, J. A., Lapshov, I., & Kaaret, P. 1998, *ApJ*, 494, 747, doi: [10.1086/305240](https://doi.org/10.1086/305240)
- Veledina, A., Muleri, F., Poutanen, J., et al. 2023a, arXiv e-prints, arXiv:2303.01174, doi: [10.48550/arXiv.2303.01174](https://doi.org/10.48550/arXiv.2303.01174)
- . 2023b, arXiv e-prints, arXiv:2303.01174, doi: [10.48550/arXiv.2303.01174](https://doi.org/10.48550/arXiv.2303.01174)
- Weisskopf, M. C., Soffitta, P., Baldini, L., et al. 2022, *Journal of Astronomical Telescopes, Instruments, and Systems*, 8, 026002, doi: [10.1117/1.JATIS.8.2.026002](https://doi.org/10.1117/1.JATIS.8.2.026002)
- West, A., & Krawczynski, H. 2023, *ApJ*
- Zhang, W., Dovčiak, M., & Bursa, M. 2019, *ApJ*, 875, 148, doi: [10.3847/1538-4357/ab1261](https://doi.org/10.3847/1538-4357/ab1261)